

# ESD STRESS ANALYSIS AND SUPPRESSION IN A SINGLE-JUNCTION THERMAL CONVERTER

Thato Ernest KGAKATSI<sup>1,2</sup> , Eugene GOLOVINS<sup>2</sup> , Johan VENTER<sup>1</sup> 

<sup>1</sup>Department of Electrical and Electronic Engineering Technology,  
Faculty of Engineering & the Built Environment, University of Johannesburg,  
Auckland Park, Johannesburg, South Africa

<sup>2</sup>National Metrology Institute of South Africa, Meiring Naude Road, Pretoria, South Africa

tkgakatsi@nmisa.org, egolovins@gmail.com, johanv@uj.ac.za

DOI: 10.15598/aeec.v20i1.4115

Article history: Received Feb 22, 2021; Revised Nov 15, 2021; Accepted Jan 01, 2022; Published Mar 31, 2022.  
This is an open access article under the BY-CC license.

**Abstract.** This article presents an outline of Electric Transient Disturbances (ETDs), represented by the ElectroStatic Discharge (ESD) in accordance with the Human-Body Model (HBM), on the AC-DC transfer measurement standard, represented by the Single-Junction Thermal Converter (SJTC) Thermal Element (TE). Mitigation technique against the power dissipation build-up, higher than the operational margins recommended by a manufacturer, on the TE were proposed and modelled using Laplace Transform (LT) analysis. A mathematical model and an optimization algorithm were developed to determine the equivalent circuit model parameters of a Transient Overload Protection Module (TOPM) that would offer adequate protection against destructive power dissipation levels build-up on the TE. The mathematical model was developed using an 8 kV ESD, which was expected to deliver short-circuit current with a peak value of approximately 5.33 A through a load impedance of approximately 1 m $\Omega$ . The ESD stress signal was injected into the TOPM connected in parallel with the TE. The active power dissipated by the SJTC TE per period of transient response was calculated from the current and voltage obtained from the mathematical analysis, and the results indicate a power dissipation of 10 mW by the TE. From the algorithm, the model parameter that noticeably influences the power dissipation capabilities of the TOPM is the inductance and it must be smaller than 1.2 nH. A CAD based simulation model was developed and analysed. The simulation results agreed with the mathematical model.

## Keywords

*Electromagnetic transients, electrostatic discharges, metrology, nonlinear circuits, power dissipation.*

## 1. Introduction

The increasing trend of advancements in electronic devices has increased their susceptibility to momentary harmful voltage and current stresses [1], [2], [3], [4] and [5]. These stresses are related to ElectroStatic Discharge (ESD) and the switching mechanisms of the circuit. Injection of ESD stress into a circuit can cause a short time change in the circuit conditions, creating a transient overload (overvoltage and/or overcurrent) event [6]. A Human-Body Model (HBM), used in this work, is a component-level ESD standard that simulates a human being whose body was charged and discharged through a fingertip to a component being tested [7].

The Single-Junction Thermal Converter (SJTC) is one of the Alternating Current-Direct Current (AC-DC) transfer standards used for high-accuracy SI traceable measurements of alternating voltage [8], [9], [10], [11], [12] and [13]. The robustness of the SJTC Thermal Element (TE) is questioned when a signal of magnitude above the maximum operating threshold is injected through its input circuit [11]. In the AC-DC transfer measurement system, the ESD stress could be generated by laboratory personnel (whose clothes or body were not discharged before handling equipment)

and frequent disconnections or (re)connections of the AC-DC transfer standard to a charged cable, equipment, or measurement circuit. The sensitivity of an SJTC to transient overload stress requires the implementation of a transient overload protection measure. Devices having the properties of fast response, high energy absorption capability, and absolute discreteness are desired.

The study of HBM ESD signals in the SJTC and implementation of transient overload stress mitigation methods is important to always ensure the standard's calibration state and safety. In this paper, mathematical models are developed using Laplace Transform (LT) techniques to determine the response of a 5 mA rated SJTC (with 90  $\Omega$  heater resistance) and a generic Transient Overload Protection Module (TOPM) to human-body ESD. CAD based simulation models are developed as part of the verification process.

## 2. Human Body Model for Electrostatic Discharge

The ESD HBM is represented by a series RLC circuit shown in Fig. 1 [1] and [2], in which  $R_{HB}$  is the human body resistance,  $L_{HB}$  is the corresponding human body inductance, required to deliver the standard waveform with specified rise time, and  $C_{HB}$  is the ability of the body to store static charges, called human body capacitance. The HBM is characterized by fast rise time (about 10 ns) and slow decay time (about 150 ns) [1].

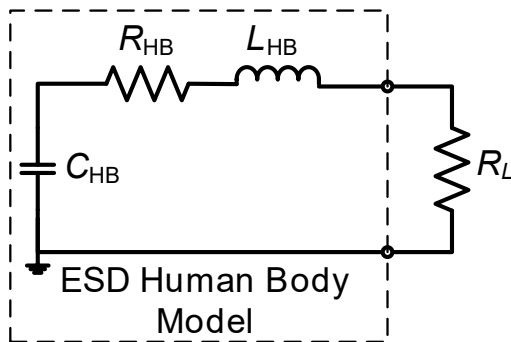


**Fig. 1:** Circuit diagram used to model the human body model of electrostatic discharge.  $R_L$  is the resistance of the device being tested.

## 3. Thermal Converter

The TE of an SJTC having a UHF pattern, presented in Fig. 2 [8], [9], [10] and [11], is a short fine resistive Nichrome heater wire with length and diameter of about 5 mm and 10  $\mu\text{m}$ , respectively [12] and [14]. Attached to the midpoint of the heater wire is a Ther-

mal Sensor (TS), a thermocouple junction, with an insulating bead, where the Seebeck effects take place and the output is measured as voltage, providing electrical isolation between the TE and TS. The TE and the TS are attached to conductive input and output support leads, respectively. A vacuum glass bulb encloses the whole structure, thus providing thermal insulation.

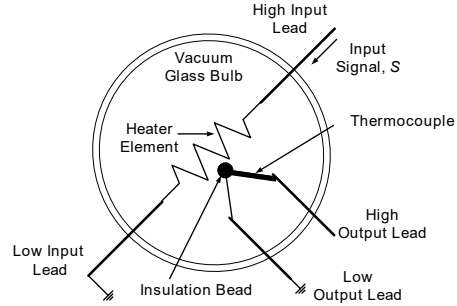


**Fig. 2:** Schematic diagram of a UHF pattern single-junction thermal converter [11] and [23].

The relationship between ac and dc signals is established by comparing the power effects produced by an unknown rms value of ac signal to those produced by a known dc signal on the TE when an electric signal is applied through the input support leads and the TE. A temperature rise (power dissipation) is generated along the TE, which is then detected by the thermocouple as the output thermal voltage (EMF) and recorded on a nanovolt detector connected to the TS through the output support leads [9], [10], [15], [16] and [17]. Since thermal resistance is inversely proportional to the cross-sectional area [18] and [19], and the support leads are of thickness greater than that of the TE, it can be deduced that Joule heating occurs almost entirely on the heater leaving support leads relatively cooler [6] and [12], therefore, power dissipation becomes negligible on the support leads. The term describing the deviation between the rms value of the ac signal and stable dc signal (owing to thermoelectric effects and frequency response of the TE) that is required to produce the same power effects in a TE, is the ac-dc transfer difference, which is expressed as [8], [12], [20], [21] and [22]:

$$\delta_{AC-DC} = \frac{S_{ac} - S_{dc}}{S_{dc}} \bigg|_{E_{ac} = \frac{1}{2}(E_{dc-} + E_{dc+})}, \quad (1)$$

where  $S_{ac}$  is the rms value of the applied ac signal,  $S_{dc}$  is the average value of the magnitudes of positive and negative applied dc signals,  $E_{ac}$  and  $E_{dc}$  are the output EMF responses to the ac and dc input signals, respectively.

For a 5 mA rated vacuum UHF-pattern SJTC, the Nichrome (80 % Ni and 20 % Cr) TE has resistance of  $R_{TE}(T_0) = 90 \Omega$ , which corresponds to the room temperature,  $T_0 = 293 \text{ K}$  [11] and [23]. This TE has a 250 % maximum input margin for safe operation,

thus it can only allow a maximum of  $I_{\max} = 12.5$  mA input current. Any current input greater than the set threshold constitutes an energy level that could potentially damage or destroy the TE. The midpoint temperature rise of the TE of this SJTC can be as high as  $T_m = 423$  K [10] and its corresponding temperature coefficient of electrical resistivity is given as  $\alpha_{TE} = +0.0001$  K<sup>-1</sup> [11]. Thus, using the known relationship between the dependence of a conductor (TE in this case) and temperature variations expressed as:

$$R_{TE}(T) = R_{TE}(T_0) (1 + \alpha_{TE}\Delta T), \quad (2)$$

where  $\Delta T = 423 - 293 = 130$  K, the resistance of this TE corresponding to the maximum temperature rise of  $T_m$  is  $R_{TE}(T_m) = 91.17 \Omega$ . The power dissipation by the TE energised to a maximum operating temperature by the maximum permissible input current is 14.25 mW, which can be calculated as:

$$P_{TE_{\max}} = I_{\max}^2 \cdot R_{TE}(T_m). \quad (3)$$

Consequently, the power dissipation by the TE energised to a maximum operating temperature  $R_{TE}(T_m)$  by the maximum permissible input voltage, i.e.,  $V_{\max} = I_{\max} \cdot R_{TE}(T_m) = 1.14$  V, is also calculated to be 14.25 mW, which is calculated as:

$$P_{TE_{\max}} = \frac{V_{\max}^2}{R_{TE}(T_m)}. \quad (4)$$

Therefore, it can be deduced from these results that the setting the input current or voltage to a value greater than 12.5 mA or 1.14 V, respectively, would generate a temperature rise greater than  $T_m$  at the midpoint of the TE. Therefore, this would cause a power dissipation greater than 14.25 mW on the TE, and could result in damage or complete destruction [23].

## 4. Modelling and Results Discussion

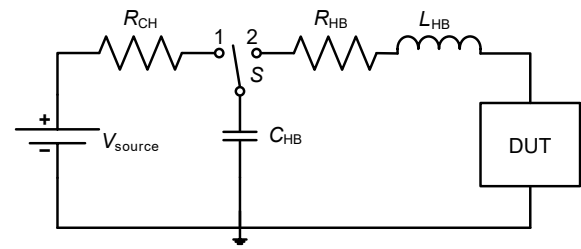
The process of this study is outlined below:

- development of the mathematical model through derivation and analysis, discussed in detail in Subsec. 4.1. ,
- implementation of the application model in CAD based simulation and analysis, discussed in detail in Subsec. 4.2.

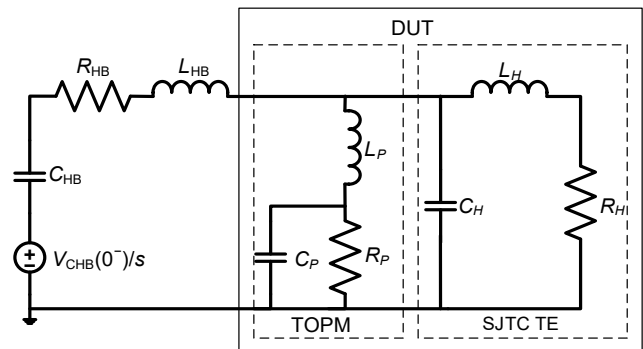
### 4.1. Mathematical Modelling Results and Discussion

Presented in Fig. 3(a) is the test setup for the ESD application in accordance with HBM to sensitive com-

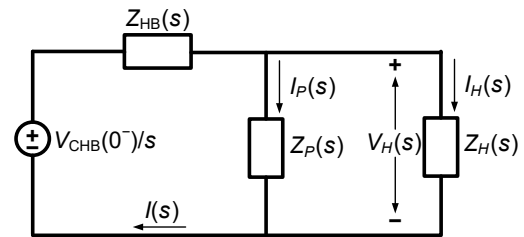
ponents. In this section, the Device-Under-Test (DUT) is a combination of a SJTC input circuit and a TOPM generic circuit model shunt at the input of the SJTC circuit. The application model in Fig. 3(b) shows that the SJTC input is modelled using an electrical equivalent circuit which represents a parallel connection of the capacitance ( $C_H$ ) and a series of inductance ( $L_H$ ) and resistance ( $R_H$ ) [10], [11], [14] and [24], whereas, the TOPM is modelled using a generic equivalent circuit model which represents series connection of the inductance ( $L_P$ ) and a parallel of capacitance ( $C_P$ ) and resistance ( $R_P$ ). The application model in the LT domain is shown in Fig. 3(c).



(a) ESD test model.



(b) Application model.



(c) Application model in LT domain.

**Fig. 3:** Circuit model for the analysis of electrostatic discharge current and voltage across the single-junction thermal converter heater.

The determination of the TOPM equivalent circuit model parameters which would be adequate to prevent the build-up of the power dissipation in the SJTC to a destructive level, which exceeds the maximum rating indicated in the manufacturer’s specification, is carried out using the following steps:

*Step 1:* analysis of the current through the SJTC and voltage at the input using LT.

*Step 2:* taking the Inverse Laplace Transform (ILT) of the current and voltage, obtained in step 1, and calculation of the active power dissipated over the duration of the transient response.

*Step 3:* optimization of the power dissipation time function.

The circuit model parameters of a complete application model network (Fig. 3(b)) are [1], [2], [11] and [13]:

HBM:  $V_{\text{CHB}}(0^-) = V_{\text{ESD}} = 8 \text{ kV}$ ,  $C_{\text{HB}} = 100 \text{ pF}$ ,  $R_{\text{HB}} = 1.5 \text{ k}\Omega$ , and  $L_{\text{HB}} = 7.5 \text{ }\mu\text{H}$ .

SJTC TE:  $C_H = 0.3 \text{ pF}$ ,  $R_H = 90 \text{ }\Omega$ , and  $L_H = 26 \text{ nH}$ .

The  $90 \text{ }\Omega$  SJTC TE is rated for  $5 \text{ mA}$  current, thus voltage rating is  $0.45 \text{ V}$  [11]. It has  $250 \%$  maximum permissible load, therefore,  $12.5 \text{ mA}$  and  $1.125 \text{ V}$  set the current and voltage threshold marks, respectively, which corresponds to a  $14.25 \text{ mW}$  power dissipation.

TOPM:  $C_P = 10 \text{ pF}$ ,  $R_P = 100 \text{ m}\Omega$ , and  $L_P = 1 \text{ nH}$  are selected to meet the protection requirements of the SJTC TE.

Assuming that at  $t < 0$ , switch  $S$  (Fig. 3(a)) is in position 1,  $C_{\text{HB}}$  is charged to the desired voltage level through the charging resistor,  $R_{\text{CH}}$ . At the instance  $t = 0$ ,  $S$  is moved to position 2 and  $C_{\text{HB}}$  is discharged onto the DUT circuit through  $R_{\text{HB}}$  and  $L_{\text{HB}}$ . TOPM is assumed to be activated instantaneously at  $t = 0$ ; however, real-world TOPM devices (TVS devices) tend to have the latency to open after the excessive voltage is sensed at their terminals. The conditions for the current through the inductors and the voltage across capacitors in a complete application model network are:

$$\begin{aligned} i_{L_{\text{HB}}}(0^-) &= i_{L_P}(0^-) = i_{L_H}(0^-) = 0, \\ i_{L_{\text{HB}}}(0) &= i_{L_P}(0) = i_{L_H}(0) = 0, \\ v_{C_{\text{HB}}}(0^-) &= v_{C_{\text{HB}}}(0) = V_{\text{ESD}}, \\ v_{C_P}(0^-) &= v_{C_H}(0^-) = v_{C_P}(0) = v_{C_H}(0) = 0. \end{aligned} \quad (5)$$

Using these conditions and analyzing the impedance of the application circuit model (Fig. 3(b)), a circuit model in LT domain was developed (Fig. 3(c)), where the circuit impedances are:

$$\begin{aligned} Z_{\text{HB}}(s) &= R_{\text{HB}} + sL_{\text{HB}} + \frac{1}{sC_{\text{HB}}}, \\ Z_P(s) &= \frac{\frac{1}{sC_P}R_P}{\frac{1}{sC_P} + R_P} + sL_P, \\ Z_{\text{TE}}(s) &= \frac{\frac{1}{sC_H}(R_H + sL_H)}{\frac{1}{sC_H} + R_H + sL_H}. \end{aligned} \quad (6)$$

The ESD current applied to the input circuit is given by Eq. (7) and the voltage across the SJTC TE is given

by Eq. (8). Taking the ILT of Eq. (8) gives Eq. (9), where  $v_1 = 1.2 \cdot 10^{-9} \text{ V}$ ,  $v_2 = 3.9 \cdot 10^{-2} \text{ V}$ ,  $v_3 = 0.53 \text{ V}$  and  $v_4 = 2.4 \cdot 10^{-3} \text{ V}$ .

Using the voltage across the SJTC TE, as seen in Eq. (8), the current through the SJTC TE is found in LT domain as Eq. (10) and in the time domain as Eq. (11), where  $i_1 = 3.5 \cdot 10^{-10} \text{ A}$ ,  $i_2 = 1.2 \cdot 10^{-2} \text{ A}$ ,  $i_3 = 6.2 \cdot 10^{-3} \text{ A}$ ,  $i_4 = 5.9 \cdot 10^{-3} \text{ A}$ ,  $i_5 = 4.4 \cdot 10^{-5} \text{ A}$  and  $i_6 = 1.7 \cdot 10^{-2} \text{ A}$ .

The transient current flowing through the SJTC heater represents a damped sinusoid oscillation, the frequency of  $f_0 = 9.4 \text{ GHz}$ , which is determined by finding the complex poles of the current function in Eq. (11), hence, the oscillatory period is  $T_0 = 0.11 \text{ ns}$ .

The average power dissipated in the SJTC is calculated over the transient oscillatory period,  $T_0$ , as:

$$p_{H_{\text{avg}}}(t) = \frac{1}{T_0} \int_t^{t+T_0} p_H(t) dt, \quad (12)$$

where  $p_H(t) = v_H \cdot i_H$  is the instantaneous power applied to the input of the SJTC. The transient response observation time is determined as the largest time constant,  $T_m$ , in the overall RLC network:

$$\begin{aligned} T_m &= \max(\tau_{C_{\text{HB}}}, \tau_{C_P}, \tau_{C_H}, \tau_{L_{\text{HB}}}, \tau_{L_P}, \tau_{L_H}) = \\ &= 0.15 \text{ }\mu\text{s}, \end{aligned} \quad (13)$$

with time constants:

$$\begin{aligned} \tau_{C_{\text{HB}}} &= C_{\text{HB}} \left( R_{\text{HB}} + \frac{R_P R_H}{R_P + R_H} \right), \\ \tau_{C_P} &= C_P \left( \frac{R_{\text{HB}} R_P R_H}{R_{\text{HB}} R_P + R_{\text{HB}} R_H + R_P R_H} \right), \\ \tau_{C_H} &= C_H \left( \frac{R_{\text{HB}} R_P R_H}{R_{\text{HB}} R_P + R_{\text{HB}} R_H + R_P R_H} \right), \\ \tau_{L_{\text{HB}}} &= L_{\text{HB}} \left( R_{\text{HB}} + \frac{R_P R_H}{R_P + R_H} \right)^{-1}, \\ \tau_{L_P} &= L_P \left( R_P + \frac{R_{\text{HB}} R_H}{R_{\text{HB}} + R_H} \right)^{-1}, \\ \tau_{L_H} &= L_H \left( R_H + \frac{R_P R_{\text{HB}}}{R_P + R_{\text{HB}}} \right)^{-1}. \end{aligned} \quad (14)$$

The results for the periodical damped oscillations and transient response settling in the SJTC load are shown in Fig. 4 and Fig. 5, respectively.

The last step is to determine the maximum power dissipated in the SJTC (Fig. 6). Optimization algorithm that searches for the global maximum of the active power response was proposed as follows:

*Step 1:* count number of oscillation periods up to the point where power peaks,

*Step 2:* double this value to set time variable range over which search will be performed,

$$I(s) = \frac{V_{ESD}}{s} \frac{Z_P(s) + Z_H(s)}{Z_P(s)Z_{HB}(s) + Z_H(s)Z_{HB}(s) + Z_P(s)Z_H(s)}, \quad (7)$$

$$V(s) = \frac{V_{ESD}}{s} \frac{Z_H(s)}{Z_{HB}(s) + Z_H(s) + Z_{HB}(s)Z_H(s)Z_P^{-1}(s)}, \quad (8)$$

$$v_H(t) = v_1 e^{-1 \cdot 10^{12}t} - v_2 e^{-3.3 \cdot 10^9t} + v_3 \left( e^{-1.9 \cdot 10^8t} + e^{-6.9 \cdot 10^6t} \right) - \left( \cos(5.9 \cdot 10^{10}t) + v_4 \sin(5.9 \cdot 10^{10}t) \right) e^{-1.1 \cdot 10^8t}, \quad (9)$$

$$I_H(s) = \frac{V_{ESD}}{s} \frac{1}{Z_{HB}(s) + Z_H(s) + Z_{HB}(s)Z_H(s)Z_P^{-1}(s)}, \quad (10)$$

$$i_H(t) = -i_1 e^{-1 \cdot 10^{12}t} - i_2 e^{-3.3 \cdot 10^9t} + i_3 e^{-1.9 \cdot 10^8t} + i_4 e^{-6.9 \cdot 10^6t} + \left( -i_5 \cos(5.9 \cdot 10^{10}t) - i_6 \sin(5.9 \cdot 10^{10}t) \right) e^{-1.1 \cdot 10^8t}, \quad (11)$$

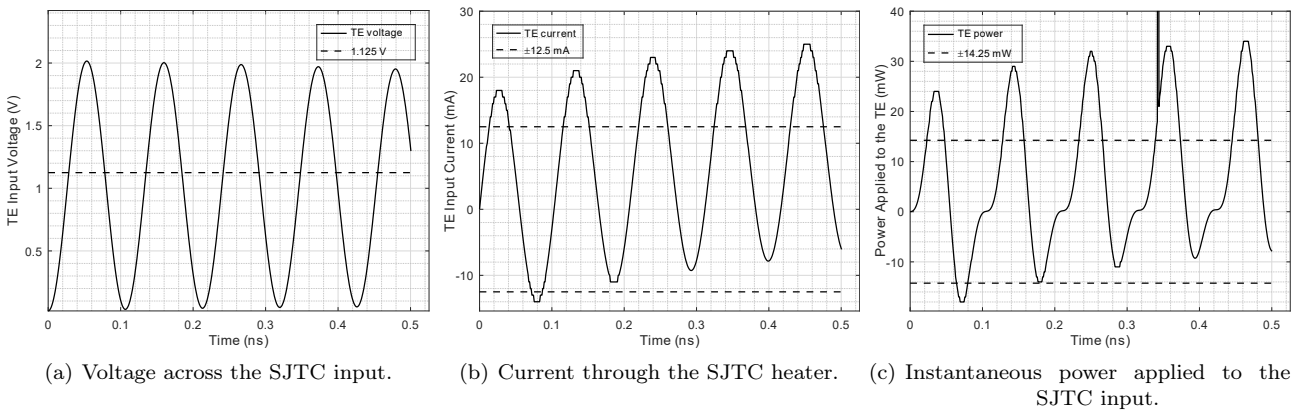


Fig. 4: Results for damped oscillations in the SJTC load.

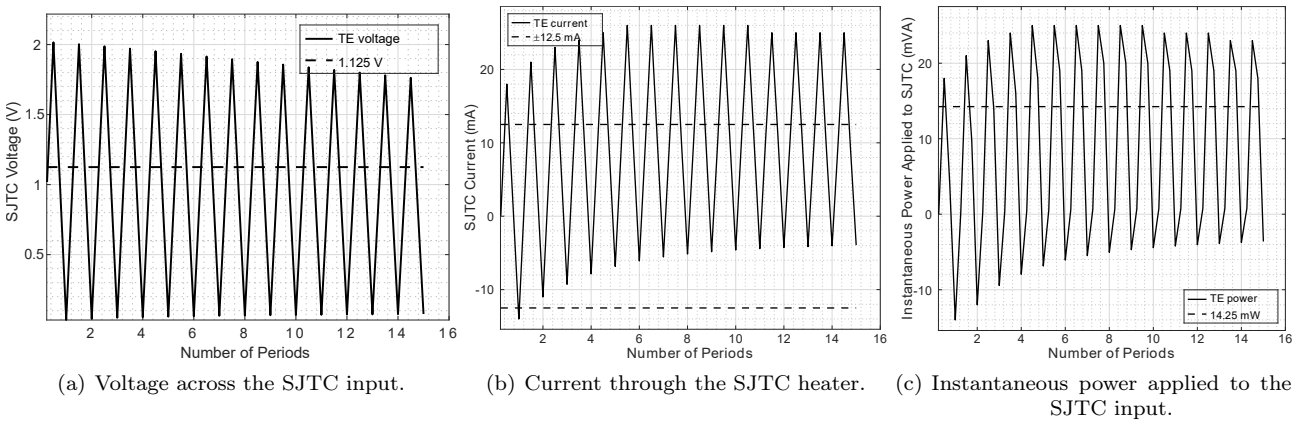


Fig. 5: Results for the transient response settling observed in the SJTC load.

Step 3: perform linear interpolation of a power function with 4 equidistant line sections for the entire time range to smoothen ripple of the function curve,

Step 4: decrement step size (i.e., increment number of line sections) and perform interpolation again, repeat while a number of zero crossings by the gradient function does not exceed unity,

Step 5: calculate time value corresponding to the last line section, at the ends of which zero-crossings were detected.

From the algorithm, the maximum average power dissipated is found to be  $p_{H_{avg}} = 10 \text{ mW}$ , corresponding to a maximum time of  $t_{max} = 0.82 \text{ ns}$ .

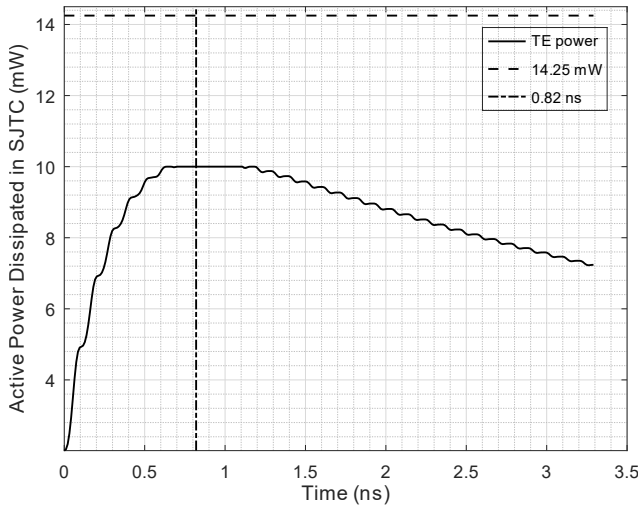


Fig. 6: Power dissipated in a SJTC heater.

### 4.2. CAD Based Simulation Results and Discussion

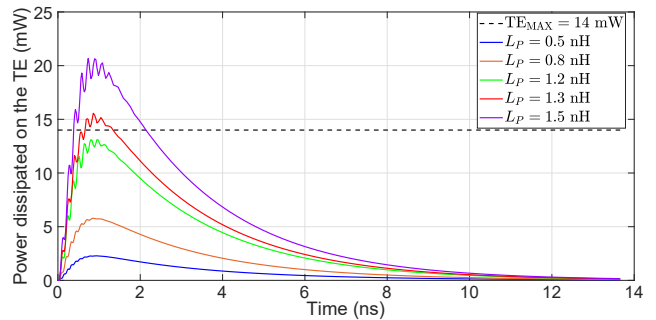
The application model shown in Fig. 3(b) was simulated with the same parameters as described in Subsec. 4.1. ; however, the TOPM model parameters were varied to determine their influence on the protection of the SJTC. The TOPM model parameters were simulated as:  $L_P$  values were 0.5 nH, 0.8 nH, 1.2 nH, 1.3 nH and 1.5 nH, while keeping  $R_P$  and  $C_P$  constant for each parametric sweep. Initially  $R_P = 10 \text{ m}\Omega$  and  $C_P = 10 \text{ pF}$ , then  $R_P = 100 \text{ m}\Omega$  and  $C_P = 10 \text{ pF}$ , and lastly  $R_P = 100 \text{ m}\Omega$  and  $C_P = 1000 \text{ pF}$ . The power dissipated by the SJTC for each parameter sweep is presented in Fig. 7(a), Fig. 7(b) and Fig. 7(c).

From the simulation results presented in Fig. 7, it can be noted that the value of  $L_P$  has a noticeable influence on the power dissipation by the SJTC.  $R_P$  has an influence on the duration of signal decay, whereas  $C_P$  has no effect on the performance of the SJTC.

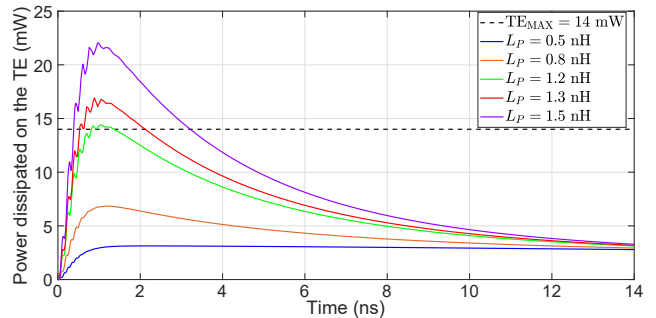
### 4.3. Analysis and Discussion of Design Trends

With the power function optimization, marginal value sets for TOPM parameters were analyzed for conformance with the limit on the power dissipated in SJTC heater (250 % of the rated current of 5 mA) as shown in Tab. 1. These marginal values are known to be inherent to real-world TOPM devices.

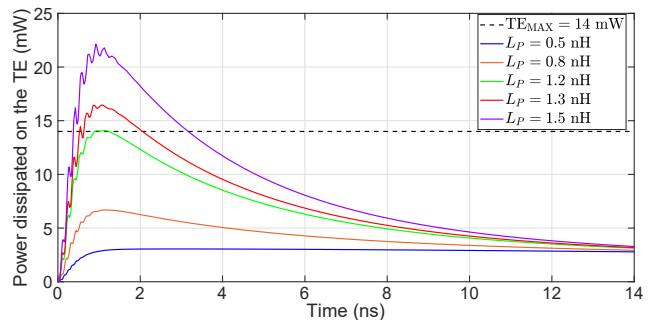
Fig. 8 shows the influence of TOPM inductance and resistance on the power dissipation by the SJTC, which



(a)  $R_P = 10 \text{ m}\Omega$  and  $C_P = 10 \text{ pF}$ .



(b)  $R_P = 100 \text{ m}\Omega$  and  $C_P = 10 \text{ pF}$ .



(c)  $R_P = 100 \text{ m}\Omega$  and  $C_P = 1000 \text{ pF}$ .

Fig. 7: Results for power dissipated in a SJTC heater simulated by varying  $L_P$  values while keeping  $R_P$  and  $C_P$  constant.

are represented by Eq. (15), where:  $vL = \begin{pmatrix} 0.5 \\ 1 \\ 1.5 \end{pmatrix}$ ,  
 $vP_{10 \text{ m}\Omega} = \begin{pmatrix} 0.0023 \\ 0.0092 \\ 0.021 \end{pmatrix}$ , and  $vP_{100 \text{ m}\Omega} = \begin{pmatrix} 0.0031 \\ 0.01 \\ 0.022 \end{pmatrix}$ .

With the adopted generic TOPM model,  $L_P$  is the only parameter which noticeably influences energy absorption by the TOPM device.  $R_P$  should be designed to be as low as possible to ensure adequate shorting performance. If  $R_P$  is orders of magnitude less than SJTC resistance, the peak power dissipation is not influenced. Higher  $R_P$  values facilitate larger time constants and can, therefore, defer the peak in time that might be useful to account for TOPM opening latency. However, this observation holds true only if  $L_P$  value is small enough (an order of pH), thus limiting the prac-

$$\begin{aligned} P_{10\text{ m}\Omega}(L) &= \text{interp}(1\text{spline}(vL, vP_{10\text{ m}\Omega}), vL, vP_{10\text{ m}\Omega}, L), \\ P_{100\text{ m}\Omega}(L) &= \text{interp}(1\text{spline}(vL, vP_{100\text{ m}\Omega}), vL, vP_{100\text{ m}\Omega}, L). \end{aligned} \quad (15)$$

**Tab. 1:** Analysis of TOPM parameter marginal values for power dissipation conformance.

$R_P$ (m $\Omega$ )	$C_P$ (pF)	$L_P$ (nH)	$t_{\max}$ (ns)	$p_{H_{\text{avg}}}$ (mW)
10	10	0.5	0.66	2.3
		1	0.57	9.2
		1.5	0.64	21
100	10	0.5	1.9	3.1
		1	0.82	10
		1.5	0.68	22
100	1000	0.5	2.8	3.1
		1	0.76	10
		1.5	0.69	22

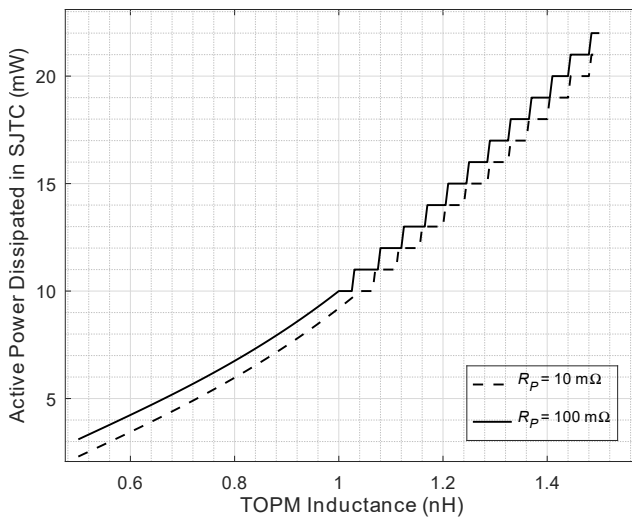


**Fig. 8:** Power dissipated in a SJTC heater as a function of the TOPM inductance.

tical relevance.  $C_P$  was found to have no impact on the transient response power curve. Similar to  $R_P$ ,  $C_P$  value has an ability to delay power peak if  $L_P$  is in the small values range.  $L_P$  value has to be smaller than 1.2 nH to prevent overload of the SJTC. Transient peak power drops rapidly with  $L_P$  decreasing below 1 nH. Leads and connectors contribute to inductance; therefore, TOPM shunting design should be as compact as possible.

## 5. Conclusion

In this work, the operation principle and architecture of the single-junction thermal converter were outlined. A mitigation technique by the implementation of TVS devices was introduced, modelled and analysed. A mathematical model for a generic transient overload protection device was developed and modelled in order to establish the protection device design targets to satisfy the protection margins of the TE. The active power

dissipated by the SJTC TE per period of transient response was calculated from the current and voltage obtained from the mathematical analysis, and the results indicated a power dissipation of 10 mW by the TE, which is below the SJTC maximum power dissipation threshold value of a 14.25 mW. A CAD based simulation model was developed, modelled and analysed to verify the mathematical model. The simulation results were in agreement with the mathematical model results. Results further indicate that the parasitic characteristics such as inductance present the limitations to the performance of the protection devices. The values of the inductance parameter must be chosen to be smaller than 1.2 nH.

## Acknowledgment

Special thanks go to the National Metrology Institute of South Africa Physical and Electrical Metrology division for the provided resources and support.

## Author Contributions

T.E.K. developed the theoretical formalism under supervision of J.V. and E.G. T.E.K. and E.G. performed the analytic calculations and performed the numerical simulations. T.E.K., J.V. and E.G. contributed to the final version of the manuscript. J.V. and E.G. supervised the project.

## References

- [1] WANG, A. Z. H. ESD Test Models. In: *On-Chip ESD Protection for Integrated Circuits*. 1st ed. Boston: Springer, 2002, pp. 11–34. ISBN 978-0-306-47618-1.

- [2] Onsemi. Human Body Model (HBM) vs. IEC 61000-4-2. TND410/D. In: *onsemi* [online]. 2010. Available at: <https://www.onsemi.jp/PowerSolutions/document/TND410-D.PDF>.
- [3] KGAKATSI, T. E., E. GOLOVINS, J. VENTER and D. V. NICOLAE. Protection against transient overvoltage in precision AC-DC transfer measurement system. In: *Fifth Conference on Sensors, MEMS, and Electro-Optic Systems*. Skukuza: SPIE, 2019, pp. 327–332. DOI: 10.1117/12.2501142.
- [4] CHO, S., D. LEE, I. ALI, S. KIM, Y. PU, S. YOO and K. LEE. Highly reliable automotive integrated protection circuit for human body model ESD of +6 kV, over voltage, and reverse voltage. *Electronic Letters*. 2017, vol. 53, iss. 13, pp. 843–845. ISSN 1350-911X. DOI: 10.1049/el.2017.0780.
- [5] LAN, T.-Y., S.-L. CHEN, H.-W. CHEN and Y.-M. LEE. Research on ESD Protection of Ultra-High Voltage nLDMOS Devices by Super-Junction Engineering in the Drain-Side Drift Region. *IEEE Journal of the Electron Devices Society*. 2021, vol. 9, iss. 1, pp. 763–773. ISSN 2168-6734. DOI: 10.1109/JEDS.2021.3102278.
- [6] NEASCU, O., O. BENIUGA, S. URSACHE and M. PAULET. Modelling and analysis the current pulse associated with electrostatic discharges. In: *2012 International Conference and Exposition on Electrical and Power Engineering*. Iasi: IEEE, 2012, pp. 585–590. ISBN 978-1-4673-1172-4. DOI: 10.1109/ICEPE.2012.6463871.
- [7] YANG, L., C. YANG, Y. TU, X. WANG and Q. WANG. Field-Circuit Co-Simulation Method for Electrostatic Discharge Investigation in Electronic Products. *IEEE Access*. 2021, vol. 9, iss. 1, pp. 33512–33521. ISSN 2169-3536. DOI: 10.1109/ACCESS.2021.3061125.
- [8] SILCOCKS, A. H. *Electronics Testing & Measurement: Measurement of a.c. Values*. 1st ed. London: Macmillan Engineering Evaluations, 1972. ISBN 978-1-349-01191-9.
- [9] ALI, R. S. M. Comparison between two different designs in the AC voltage measurement. *Measurement*. 2011, vol. 44, iss. 9, pp. 1539–1542. ISSN 1873-412X. DOI: 10.1016/j.measurement.2011.06.005.
- [10] HERMACH, F. L. AC-DC comparators for audio-frequency current and voltage measurements of high accuracy. *IEEE Transactions on Instrumentation and Measurement*. 1976, vol. 25, iss. 4, pp. 489–494. ISSN 1557-9662. DOI: 10.1109/TIM.1976.6312271.
- [11] WIDDIS, F. C. The theory of Peltier- and Thomson-effect errors in thermal a.c.-d.c. transfer devices. *Proceedings of the IEE - Part C: Monographs*. 1962, vol. 109, iss. 16, pp. 328–334. ISSN 2054-0426. DOI: 10.1049/pi-c.1962.0048.
- [12] Best technology International, Inc. Vacuum Thermocouples. In: *besttech* [online]. 2022. Available at: <http://besttech.com/index.htm>.
- [13] BUBANJA, V. The ac-dc difference of single-junction thermal converters. *Journal of Engineering Mathematics*. 2000, vol. 38, iss. 1, pp. 33–50. ISSN 0022-0833. DOI: 10.1023/A:1004637514734.
- [14] HERMACH, F. L. and E. S. WILLIAMS. Thermal Converters for Audio-Frequency Voltage Measurements of High Accuracy. *IEEE Transactions on Instrumentation and Measurement*. 1966, vol. 15, iss. 4, pp. 260–268. ISSN 1557-9662. DOI: 10.1109/TIM.1966.4313549.
- [15] HALAWA, M. and N. AL-RASHID. Performance of Single Junction Thermal Voltage Converter (SJTVC) at 1 MHz via Equivalent Electrical Circuit Simulation. In: *2010 12th International Conference on Computer Modelling and Simulation*. Cambridge: IEEE, 2010, pp. 631–636. ISBN 978-1-4244-6615-3. DOI: 10.1109/UKSIM.2010.120.
- [16] AMAGAI, Y. and Y. NAKAMURA. Numerical analysis of low-frequency properties in single-junction thermal converters. *IEEJ Transactions on Electrical and Electronic Engineering*. 2012, vol. 7, iss. 4, pp. 350–354. ISSN 1931-4981. DOI: 10.1002/tee.21739.
- [17] HERNANDEZ-PRADA, C. F., M. SACHICAVELLANEDA and A. MARTINEZ-LOPEZ. High accuracy AC current sources calibration by single junction thermal converters at INM. *DYNA*. 2021, vol. 88, iss. 216, pp. 117–125. ISSN 2346-2183. DOI: 10.15446/dyna.v88n216.86244.
- [18] JHA, C. M., M. A. HOPCROFT, M. AGARWAL, S. A. CHANDORKAR, R. N. CANDLER, V. SUBRAMANIUN, R. MELAMUD, S. BHAT, B. KIM, K. K. PARK and T. W. KENNY. In-Chip Device-Layer Thermal Isolation of MEMS Resonator for Lower Power Budget. In: *ASME 2006 International Mechanical Engineering Congress and Exposition*. Chicago: ASME, 2006, pp. 97–103. ISBN 0-7918-4775-6. DOI: 10.1115/IMECE2006-15176.
- [19] LOBONTIU, N. Fluid and Thermal Systems. In: *System Dynamics for Engineering Students*. 1st ed. Burlington: Elsevier Inc., 2010, pp. 151–203. ISBN 978-0-08-092842-5.

- [20] AMAGAI, Y. and H. FUJIKI. Improved Electrothermal Simulation for Low-Frequency Characterization of a Single-Junction Thermal Converter. *IEEE Transactions on Instrumentation and Measurement*. 2014, vol. 63, iss. 12, pp. 3011–3018. ISSN 1557-9662. DOI: 10.1109/TIM.2014.2313952.
- [21] SAEED, T. S., M. HALAWA, I. A. ELRAHMAN and A. S. ELDIN. Electrical Modeling and Simulation of AC-DC Thermal Transfer Devices to Investigate the Errors Sources. In: *2018 Conference on Precision Electromagnetic Measurements (CPEM 2018)*. Paris: IEEE, 2018, pp. 1–2. ISBN 978-1-5386-0974-3. DOI: 10.1109/CPEM.2018.8501189.
- [22] AMAGAI, Y., M. MARUYAMA and H. FUJIKI. Low-Frequency Characterization in Thermal Converters Using AC-Programmable Josephson Voltage Standard System. *IEEE Transactions on Instrumentation and Measurement*. 2013, vol. 62, iss. 6, pp. 1621–1626. ISSN 1557-9662. DOI: 10.1109/TIM.2013.2245182.
- [23] KGAKATSI, T. E. *Overload Protection for AC-DC Transfer Measurement Standards*. Johannesburg, 2020. Master Thesis. University of Johannesburg. Supervisor Johan Venter.
- [24] NOVAKOVA-ZACHOVALOVA, V., S. MASLAN, M. SIRA and J. STREIT. Development of primary standard for ac-dc current transfer difference. In: *2016 Conference on Precision Electromagnetic Measurements (CPEM 2016)*. Ottawa: IEEE, 2016, pp. 1–2. ISBN 978-1-4673-9134-4. DOI: 10.1109/CPEM.2016.7540674.

## About Authors

**Thato Ernest KGAKATSI** was born in Zeerust town, South Africa. He received his M.Phil. in

Electrical and Electronic Engineering (with distinction) from University of Johannesburg, South Africa, B.Sc. Honours in Physical Sciences from University of the Western Cape, South Africa, and B.Sc. with Electronics and Physics as majors from North-West University, South Africa, in 2020, 2018 and 2016, respectively. He published one conference paper. His research interests include transient overvoltage and overcurrent in low-voltage and low-power electronics, applications of transient overload protection devices, and electrical AC metrology.

**Eugene GOLOVINS** was born in Riga, Latvia. He received his Ph.D. in Electrical Engineering from the University of Cape Town in 2010. His recent research experience lies in the area of test and measurement engineering with application to the low-frequency instrumentation and sensor electronics. Since February 2013, he has been a research and calibration engineer in the precision AC measurements laboratory. His main duties are design, integration, and validation of the automated precision AC measurement systems. He is an author of several journal and conference publications and a senior member of IEEE.

**Johan VENTER** was born in Pretoria, South Africa. He completed his B.Eng. Electronic Engineering, B.Eng. (Hons) Electronic Engineering, M.Eng. Microelectronic Engineering and Ph.D. Electronic Engineering in 2009, 2010, 2013 and 2020 respectively at the University of Pretoria. In 2014 he joined the University of Johannesburg as a lecturer in the Department of Electrical and Electronic Engineering Technology and was promoted to senior lecturer in 2020 after the conferral of his Ph.D. He teaches various modules (undergraduate and Honors level) and actively supervises postgraduate students. He authored or co-authored 9 conference articles and 3 journals. He holds a membership with IEEE. His research interests include readout circuitry in CMOS based microelectronics and sensor technologies.